Interface and Strain Effects on the Thermal Conductivity of Heterostructures: A Molecular Dynamics Study

Alexis R. Abramson

Chang-Lin Tien

Arun Majumdar
e-mail: majumdar@me.berkeley.edu

Department of Mechanical Engineering,
University of California,
Berkeley, CA 94720-1740

Molecular dynamics simulations are used to examine how thermal transport is affected by the presence of one or more interfaces. Parameters such as film thickness, the ratio of respective material composition, the number of interfaces per unit length, and lattice strain are considered. Results indicate that for simple nanoscale strained heterostructures containing a single interface, the effective thermal conductivity may be less than half the value of an average of the thermal conductivities of the respective unstrained thin films. Increasing the number of interfaces per unit length, however, does not necessarily result in a corresponding decrease in the effective thermal conductivity of the superlattice.
[DOI: 10.1115/1.1495516]

Keywords: Conduction, Heat Transfer, Microscale, Molecular Dynamics, Nanoscale, Thin Films

Introduction

As the demand for miniaturization of microelectronics devices increases, superior thermal control becomes even more important to the future success of the microelectronics and other industries. Reduced feature sizes lead to an increase in power dissipation per unit area, and therefore thermal management is a major concern. However, research in this area has shown that thermal behavior in micro/nano-sized devices often cannot be predicted by conventional macroscopic theory. Nonetheless, the discovery of unique micro/nanoscale thermal phenomena has led to an interest in new devices and applications that take advantage of the unusual physics, and in particular has stimulated new research in the area of thermoelectrics [1,2]. An efficient thermoelectric device must maximize the ratio of electrical to thermal conductivity in addition to providing a high Seebeck coefficient. Hence, engineering a material with a low thermal conductivity is one manner in which to improve the functionality of the device. The ability to predict, control and manipulate the thermal transport in micro/nanostructures will most likely result in future progress in the area of thermoelectrics.

One of the first observations of unusual thermal characteristics of micro/nanostructures involved the appearance of a reduced thermal conductivity in superlattices [3,4], which are two-dimensional structures of alternating thin films. Capinski et al. [5,6] demonstrated that the thermal conductivity of GaAs/AlAs superlattices can be less than that of an alloy of the two materials. Lee et al. [7] also reported a reduced thermal conductivity associated with Si/Ge superlattices. They showed there is an increase in thermal conductivity with period thickness, resulting in a peak at ~200 Å, followed by a significant downward trend. In contrast, Yamasaki et al. [8] and Venkatasubramanian et al. [9] discovered the opposite trend in Bi_2Te_3/Sb_2Te_3 superlattices; for periods shorter than 60 Å, the thermal conductivity of these heterostructures actually *decreases* with increasing period thickness, followed by a trend of *increasingly* higher values. Moreover, Huxtable et al. studied $Si/Si_{0.7}Ge_{0.3}$ superlattices and uncovered no peak in thermal conductivity; rather, they revealed a non-linear decrease with decreasing period thickness from 300 Å to 45 Å [10]. Some investigations suggest that interface quality may also significantly affect the thermal conductivity of superlattices [11,12]. However, researchers have reported seemingly contradictory experimental results regarding the effect of interface roughness. In InSb/AlSb superlattices, thermal conductivity decreases as interfacial roughness becomes more pronounced [13], but the trend may be opposite for Si/Ge superlattices [14]. Although the effect of lattice strain on electronic properties in superlattices has been studied extensively over the past decade [15,16], there has been little or no research investigating how lattice strain may affect thermal conductivity in heterostructures. Theoretical studies [17–19] have demonstrated that phonon spectra are altered by strain in superlattices, but there is conflicting evidence describing the extent of the effect. Presently, questions regarding the cause of the unusual and somewhat perplexing thermal behavior in superlattices have remained unanswered. A variety of mechanisms such as acoustic impedance [20] and phonon spectra mismatch [21], mini-band formation and a corresponding phonon group velocity reduction [22–25], phonon tunneling [26], and interface scattering due to roughness, defects or dislocations [11,27] have been proposed as contributors. This work further suggests that lattice strain, commonly exhibited by symmetrically and asymmetrically strained superlattices, may also play a significant role in affecting thermal transport. There is limited understanding of these phonon heat conduction mechanisms and their relation to material properties, individual film thickness, the ratio of respective material composition, and superlattice configuration and quality. A goal of this research is to further reflect the complexity of the situation by using computer simulations to reveal interesting thermal characteristics of heterostructures.

A variety of distinctly different theoretical and computational approaches have been used to determine the effective thermal conductivity of a superlattice structure. Many studies have employed modified bulk formulas for the lattice thermal conductivity, using an appropriately adapted acoustic phonon dispersion relation for the structure [22,28]. Other investigators have applied the Boltzmann transport equation (BTE) for phonons [29,30] or Monte Carlo simulations [31,32]. Often, experimentally fitted values for the phonon relaxation time and acoustic phonon dispersion of bulk media are still employed for these methods. By including a specularity parameter in the solution of the BTE, researchers have

Contributed by the Heat Transfer Division for publication in the JOURNAL OF HEAT TRANSFER. Manuscript received by the Heat Transfer Division September 24, 2001; revision received May 13, 2002. Associate Editor: C. T. Avedisian.

been able to capture the effect of a partially diffuse interface [11,30]. This study, however, takes a different approach by using classical nonequilibrium molecular dynamics (MD) simulations to investigate the effective thermal conductivity of bi-material structures including simple representations of superlattices. Due to its classical nature, this technique cannot capture effects related to vibrational energy quantization that control heat capacity at temperatures much below the Debye temperature. However, phonon characteristics such as dispersion, interface reflection, confinement and tunneling are accurately captured without assuming empirically derived physical values, provided the interatomic potential is well known. Employing MD for this type of analysis is a less common approach, but previous research on two [33] and three-dimensional [34] superlattices using non-equilibrium and equilibrium MD techniques, respectively, have uncovered some interesting observations regarding thermal transport in superlattices.

There are various factors that may potentially influence the effective thermal conductivity of a heterostructure, including thin film thickness and the ratio of the respective material composition, numbers of interfaces, period thickness, and strain throughout the structure. This study offers a systematic examination of how these factors might influence the effective thermal conductivity and may, therefore, help to predict how to better engineer these structures for use in thermoelectric devices or other related applications. Lennard-Jones materials are simulated, and although their applicability in real applications is limited, the results should be used as a benchmark from which further study of other material systems will benefit.

Computational Model

The computational model is based on the classical MD subroutines given by Allen and Tildesley [35] and on the non-equilibrium simulations of thin films performed by Lukes et al. [36]. However, essential modifications to account for more than a single solid material have been made. A schematic of the three-dimensional molecular dynamics computational structure is shown in Fig. 1. Boundary conditions consist of an applied heat flux in the *x*-direction and are periodic over eight planes in the other two dimensions (the *y* and *z*-directions). The periodic boundary conditions simulate an infinite film in these directions, although their use does remove the existence of long-wavelength fluctuations in the system. Nonetheless, certain repeated simulations with up to four times the number of planes in each direction demonstrated no significant deviation from the results presented here. Fixed walls are used at the ends of the structure in the *x*-direction to discourage evaporation of the constituent atoms to vacuum. The heat flux is simulated by adding energy to the four planes adjacent to the leftmost fixed walls (the hot bath) and removing the same amount of energy from the four planes adjacent to the rightmost fixed walls (the cold bath). The atoms between these two baths are referred to as ''regular'' atoms. The effective cross-plane thermal conductivity of a structure is simply determined by the quotient of the heat flux and the temperature difference across the regular atoms in the structure, multiplied by the total thickness over which the thermal gradient is imposed. The instantaneous temperature at a point x is calculated classically from the planar average of the kinetic energy of the atoms in each y-z plane such that

$$T_{x,\mathrm{inst}}=\frac{m\Sigma_i^{N_x}v_i^2}{3N_xk_B} \tag{1}$$

where m is the mass and v the speed of the atom, N_x is the total number of atoms in the specific y-z plane and k_B is the Boltzmann constant. After the simulation has reached steady state, this temperature is averaged over an adequate time period, and this time-averaged value is used in the calculation of effective thermal conductivity. An appropriate imposed heat flux is chosen for each structure to ensure that the same temperature difference (cold bath at ~60 K and hot bath at ~90 K) is maintained across all structures. Argon (Ar) and krypton (Kr) are chosen as the materials for the analysis whose Debye temperatures are approximately 92 K and 72 K and melting temperatures are approximately 84 K and 116 K, respectively. To avoid melting conditions, the Kr film, with the higher of the two melting temperatures, is always nearest the hot bath, and the simulation checks to ensure that melting does not occur. It is important to note that across this temperature range, molecular dynamics simulations have revealed that thermal conductivity is not a strong function of temperature [36], and therefore, a linear temperature profile is expected, provided the thickness of the film/structure is greater than the phonon mean free path. The actual heat flux across each plane is calculated from particle positions and velocities using the equations of Irving and Kirkwood [37]. At steady state, a time average of this calculated flux is then spatially averaged across the structure to provide an *effective* heat flux. This value can be compared with the imposed heat flux to assess the degree to which heat spreading may occur in the structure in the *y*- and *z*-directions. The total simulation time is determined by estimating the thermal diffusion time for each structure and using a run time approximately 5–20 times this characteristic time scale. Femtosecond time steps are used, and the total simulation time ranges from 1–30 nanoseconds. The probable errors of the planar temperature, the effective heat flux and the effective thermal conductivity are determined in the manner outlined in the appendix and in more detail by Lukes et al. [36]. For large structures ($\geqslant$24 unit cells in the *x*-direction), the calculated effective heat flux differed by 8–12 percent of the imposed heat flux, while for smaller structures, the value ranged between 3–8 percent. The errors in thermal conductivity reported throughout this work are associated with the convergence criteria of the simulation. For the sake of computational time, the increased accuracy of the calculation is sacrificed for large structures that may require unreasonably long simulation times. Hence, runs that are too short may be to blame for larger errors, approximately 15 percent in some cases, associated with simulating thick structures.

Utilizing a true representation of the intermolecular potential in these MD simulations is critical for ensuring that the physics underlying the micro/nanoscale thermal phenomena is accurate. Therefore, only Lennard-Jones (LJ) solids, for which the intermolecular potential is well established, are chosen. The LJ 12-6 potential is

$$\Phi(r_{ij})=4\varepsilon\left[\left(\frac{\sigma_{LJ}}{r_{ij}}\right)^{12}-\left(\frac{\sigma_{LJ}}{r_{ij}}\right)^{6}\right] \tag{2}$$

where r_{ij} is the distance between atoms i and j, ε is the well depth of the potential and σ_{LJ} is the equilibrium separation parameter. The force experienced by an atom due to the presence of another atom is simply the first derivative of Eq. (2). Using Newton's equations of motion, a relationship between force and acceleration can be established. Therefore, an indirect relation exists between the interatomic potential and the vibrational motion of the atoms in the system. Using a finite difference approach, or the com-

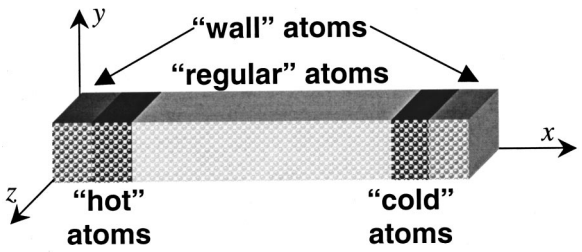

Fig. 1 Schematic of molecular dynamics simulation cell

monly employed velocity Verlet algorithm [38], the acceleration may be expressed in terms of velocity, position and time, and the solution then marches accordingly in time.

The phonon mean free path is generally less than ~2 nm in LJ materials [39] as compared to ~100 nm in "real" engineering materials such as semiconductors. Consequently, a much shorter simulation time is required to accurately capture the physics. To further reduce computation time, the common convention of using a cutoff radius outside of which atomic interactions are negligible is employed. Argon (Ar) and krypton (Kr) are chosen as the materials for the analysis because their interatomic potentials are well known. Both of these materials have a face-centered cubic unit cell (UC) structure, and therefore, one UC along the *x*-direction corresponds to two planes of atoms. Lorentz-Berthelot mixing rules [40] are used to account for interaction between Ar and Kr atoms. For simulations of bi-material films, the non-dimensional units are based on the parameters for Kr. For some simulations, a structure with a coherent interface is desired. To achieve this, the equilibrium interatomic distance is chosen for both materials to be the same and that of Kr ($a=5.64$ Å). However, the equilibrium interatomic distance for Ar is actually slightly less ($a=5.31$ Å), thereby forcing the Ar film to be in tension. By varying parameters such as structure and individual film thicknesses, the ratio of the respective material composition, the number of interfaces, and lattice strain, the simulations performed here investigate the reduction in the effective thermal conductivity of various bi-material films and simplified superlattices. Computational power limits the capability of simulating complex superlattices, but simple structures with up to twelve periods are analyzed.

For all cases, the effective thermal conductivity of the entire structure is compared to an "average" thermal conductivity using a simple series resistance calculation involving the respective resistances of the individual Ar and Kr thin films in their natural lattice states such that

$$R_{ave}=R_{Kr}+R_{Ar}$$
$$k_{ave}=\frac{(t_{Kr}+t_{Ar})k_{Kr}k_{Ar}}{t_{Kr}k_{Ar}+t_{Ar}k_{Kr}} \tag{3}$$

where R is the resistance, k is the thermal conductivity, and t is the individual film thickness. The subscript ave refers to the average property, while Kr and Ar describe the respective individual properties of each material. This equation represents the expected effective thermal conductivity if there were no interfacial thermal effects present to alter the property. Researchers often compare thermal conductivity of superlattices to an average of unstrained bulk values, assessing that the reduction in the thermal conductivity of the superlattice is due to a mechanism such as acoustic impedance mismatch. However, such a comparison may not be sufficient to further one's physical understanding of interfacial thermal effects since thin film and bulk properties may be markedly different. Therefore, this study utilizes an average of the *thin film* thermal conductivities at the appropriate corresponding temperatures for a more appropriate comparison to reveal that the interface can play a substantial role in altering thermal transport. Note that the average thermal conductivity is estimated using unstrained thermal conductivities of the individual films, which allows one to additionally compare the effect of strain in certain simulations.

Results and Discussion

Effect of Single Interface. An example of a temperature profile for a bi-material film (16 UC in the *x*-direction of Kr adjacent to 16 UC of Ar) is illustrated in Fig. 2. The temperature profiles for the simulations were reasonably linear for each individual film, and a temperature jump occurred at the interface between materials. Note that the *x*-axis corresponds to the atomic plane number, and plane number 1 corresponds to the first plane

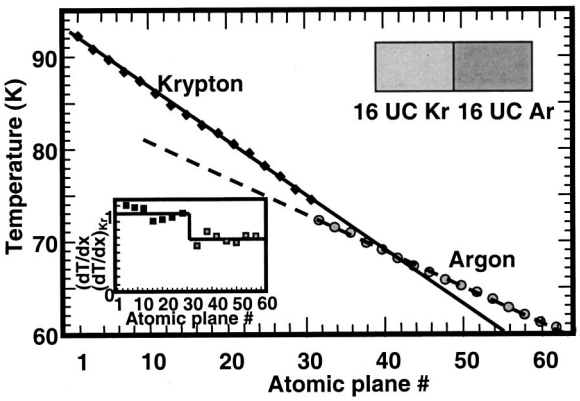

Fig. 2 One-dimensional temperature distribution from an MD simulation of a bi-material film composed of 16 unit cells Kr (solid diamond) adjacent to 16 unit cells Ar (solid circle). The temperature jump indicates the presence of interfacial thermal resistance. The inset illustrates the instantaneous and best-fit slopes of the lines corresponding to the two materials normalized using the best-fit slope of Kr.

of regular atoms adjacent to the hot bath. The best-fit lines for both the Kr and Ar halves are shown, and the respective slopes are different because the thermal properties of the materials vary. From graphs such as this one, the effective cross-plane thermal conductivity is simply determined by the ratio of the effective heat flux and the temperature difference between the first and last plane of regular atoms (using values from the best fit lines as shown) multiplied by the total thickness of the regular atoms in the structure. Since the MD simulation of a single film calculates a non-dimensional thermal conductivity for any Lennard-Jones solid, the dimensionalized values for individual films of Kr or Ar may be determined using the results from a single simulation and applying the respective transformation as given by Lukes et al. [36]. Comparing the two transformations, the dimensionalized thermal conductivity of a Kr film is theoretically about 70 percent that of Ar for any MD simulation. This is also evident from the simulations, and the normalized slopes of the two best-fit lines are illustrated on the inset to Fig. 2.

To initially assess the effect of a single interface on various thin film configurations, the thermal conductivities of lattice-strained bi-material films of differing overall thicknesses but with equal individual thicknesses of Kr and Ar are analyzed and shown in Fig. 3. The lattice strain is imposed by initially forcing the Ar

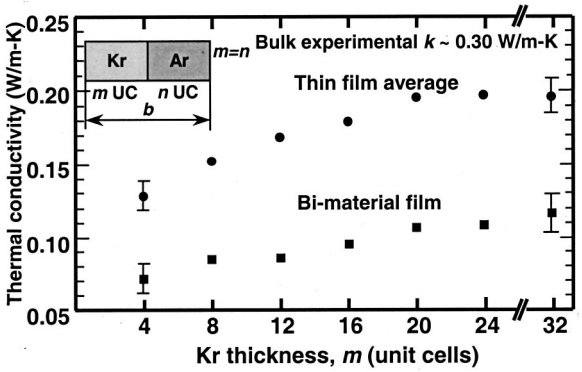

Fig. 3 Effective thermal conductivity of strained bi-material Kr/Ar films as a function of increasing thickness (solid square) and compared with thin film average (solid circle). Note $m=n$.

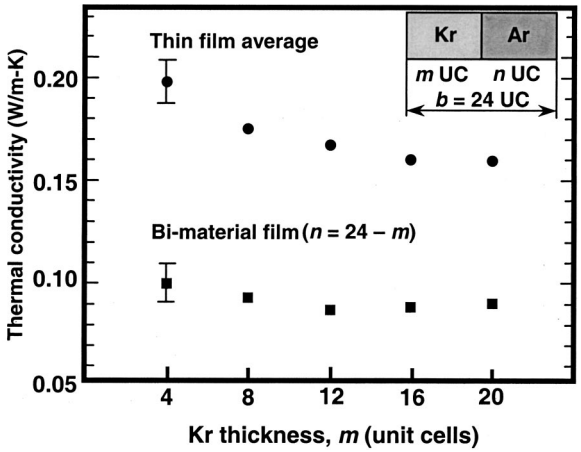

Fig. 4 Effective thermal conductivity of strained bi-material Kr/Ar films as a function of individual film thickness ratio, but the same overall thickness (solid square) and compared with thin film average (solid circle). Note $n=24-m$.

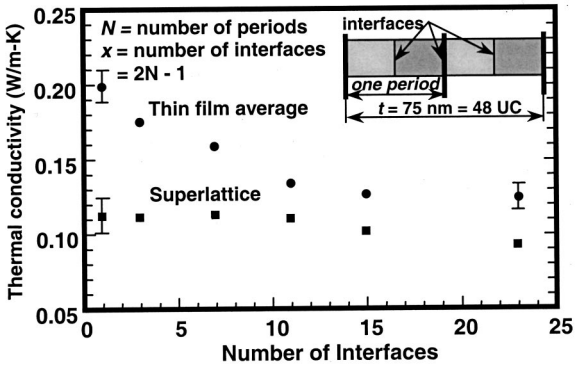

Fig. 5 Effective thermal conductivity of simple asymmetrically strained superlattices as a function of numbers of interfaces per unit thickness (solid square) and compared with thin film average (solid circle)

atoms to lattice spacings equal to that of the Kr atoms, imposing a coherent interface. Note that the structure consists of only two films and is not representative of a superlattice. The standard error analysis [36] for these simulations resulted in errors in the effective thermal conductivity between 8 and 15 percent of the calculated values. Error bars are shown for the first and last points only for clarity. The two different trends correspond to the MD simulation for the bi-material films (bottom trend) and the calculation of the ''average'' thermal conductivity (top trend). The latter assumes a simple series resistance analysis given by Eq. (3), using the MD calculated values for the individual film thermal conductivities at the appropriate corresponding temperatures. The first observation made from the data is that as individual thin film thickness increases from 4 UC to 32 UC, the effective thermal conductivity also appears to increase. The phonon mean free path of Ar is estimated to be approximately 2–3 UC [39] (and is assumed to be of the same order for Kr), and therefore boundary scattering is dominant for very thin films. Consequently, as film thickness increases, boundary effects become less pronounced, and thermal conductivity also increases. However, even for the thickest films, the thermal resistance due to interfacial effects and strain still cause a disparity between the thin film average and bi-material film values. Using the same series resistance formulation of previously reported experimental results for bulk Kr [41] and Ar [39,41], the effective thermal conductivity calculates to approximately 0.30 W/mK, which is comparable to the averaged MD results for the thicker films. Moreover, a comparison of the two trends illustrates that the presence of a single interface results in a reduction of the thermal conductivity by a factor of ~2. This discrepancy may be attributed to one or more of the thermal mechanisms responsible for interfacial thermal resistance except for the following: (i) interface scattering due to roughness, since the interface is atomically smooth, and (ii) mini-band formation, since there is no additional periodicity.

To assess the impact of the thickness ratio of the films, the effective thermal conductivities of lattice-strained bi-material films of the same overall thickness but varying thickness ratios are compared in Fig. 4. The standard error analysis for these simulations resulted in errors between 10 and 13 percent of the calculated values. For the series resistance calculation (top trend), as the amount of Ar is reduced in the structure, there is a corresponding reduction in the overall thermal conductivity since the thermal conductivity of Ar is approximately 1.4 times that of Kr. However, the decline flattens out for the 16 UC Kr/8 UC Ar and 20 UC Kr/4 UC Ar structures. It is important to recognize that there are two competing effects here: the fraction of Ar in the structure and the differences in thermal conductivities due to the disparity between film thicknesses. For example, in the 4 UC/20 UC averaged case, the structure is composed of 83 percent Ar, and the Ar film is ''thick''. Together, these effects result in a high thermal conductivity. However, for the 20 UC/4 UC averaged case, the structure is composed of only 17 percent Ar, but the thickness of the Kr film is large. Even though the thermal conductivity of Kr is theoretically 70 percent that of Ar, a 20 UC film of Kr has a thermal conductivity similar to that of a 4 UC film of Ar, and there is a flattening out of values rather than a continued decrease. There is, albeit questionably due to the relative magnitude of the results in Fig. 4, a corresponding trend for the case of the bi-material film (bottom). There is no conclusive evidence from this study that variation in the ratio of the constituent materials influences interfacial thermal effects. Nonetheless, it is important to consider this ratio in the design of engineering structures, by accounting not only for expected differences due to a disparity between thermal properties, but also for thin film boundary scattering effects if one or both of the films are of the order of or less than the phonon mean free path.

Effect of Multiple Interfaces. In engineering applications, structures consisting of multiple interfaces are often of great concern. However, there is limited understanding of how to best design a multilayer structure for superior control of thermal transport characteristics. Presently, a general rule of thumb relies on the hypothesis that increasing the number of interfaces per unit length will result in more phonons being reflected and therefore, a reduction in the effective thermal conductivity of the structure. However, some researchers have hypothesized that mini-band formation results in an overall decrease in the phonon group velocity, thereby causing a reduction in the thermal conductivity [22–25]. If this were true, increasing the numbers of interfaces per unit length would effectively decrease the period thickness, resulting in fewer locations along the dispersion relation where the group velocity approaches zero and a corresponding *increase* in thermal conductivity. Thus, if both mechanisms were significantly present, they would compete against each other to affect thermal transport. For this study, simple superlattices, all approximately 75 nm thick (48 UC), are used to assess the effect of systematically increasing the number of interfaces per unit length. The results for superlattice configurations consisting of a single interface and up to 23 interfaces (not including the boundaries) are shown in Fig. 5. This corresponds to structures comprised of one, two, four, six, eight and twelve periods but with the same overall thickness. The standard error analysis for these simulations resulted in errors in the effective thermal conductivity between 8 and 10 percent of the calculated values. The top trend in the figure, indicating the thin film average, demonstrates again that as the individual film thick-

ness decreases (as it does with increasing number of periods/interfaces), the thermal conductivity decreases. However, the superlattice thermal conductivity (bottom trend) does not significantly change over the range investigated here. Nonetheless, there appears to be a larger disparity between the thin film average and the superlattice thermal conductivity for smaller numbers of periods. This may imply that for film thicknesses much greater than the dominant phonon wavelengths, a single interface and the effect of strain may be responsible for a considerable decrease in thermal conductivity. However, adding more interfaces while maintaining the same overall thickness will not necessarily result in a large decrease in thermal conductivity if the individual film thicknesses become very small. When the thin films are of the order of the dominant phonon wavelengths, phonon tunneling may counteract any additional interface reflection effects that would otherwise result with the addition of more interfaces. Furthermore, mini-band formation may emerge when multiple periods are present, acting to further counteract any increase in interface reflection. Interestingly, some analytical predictions indicate that the thermal conductivity in superlattices should decrease with increasing period thickness due to a corresponding decrease in phonon tunneling, and then approach a constant value at a critical thickness [21,42]. However, these analytical approaches cannot entirely capture competing interfacial thermal resistance effects. There is conflicting experimental evidence that affirms but also contradicts the finding that thermal conductivity decreases with increasing period thickness [7–9], but the superlattices in the referenced experiments are of markedly different materials, qualities and configurations. Certain factors such as phonon relaxation time variation, phonon coherence and interface scattering due to roughness may differ significantly among samples and are often too complicated to evaluate, making an accurate comparison of results difficult. Although MD inherently accounts for many of these factors, limits in computational power did not permit a simple analysis of superlattices with a greater number of interfaces. Future analysis of larger superlattices may reveal interesting characteristics. For many of the superlattices fabricated and proposed as potential thermoelectric components, the thin film thicknesses may approach the order of the dominant phonon wavelengths. Even though there are many complex factors to consider, improvements in the engineering design of these structures require that at the very least, the competing effects of phonon tunneling, mini-band formation and interfacial thermal resistance be considered.

Effect of Strain. It is well known that a lattice mismatch at the interface between conducting materials can influence charge transport due to the presence of defects or misfit dislocations, and due to strain-induced changes in the electronic band structure. The effects of interfacial strain on phonon transport and thermal conductivity are not well understood. For the aforementioned MD simulations, the lattice parameter of 5.64 Å (that of Kr) was imposed on both the Kr and Ar films to ensure a coherent interface. Similar to an asymmetrically strained superlattice, the Ar film was kept in tension while the Kr film was not strained. Allowing the natural lattice state of both materials to exist during the simulations resulted in an interesting reconfiguration of the lattice structure. Figure 6 illustrates the (*a*) initial and (*b*) final atomic lattice positions in a single $x-y$ plane of a 12 UC Kr/12 UC Ar structure (only the first 12 atomic planes on either side of the interface are shown for clarity). These snapshots were taken prior to imposing a heat flux. The natural lattice constants of the respective materials were initially set in this simulation and were purposely chosen to necessitate a large and unnatural degree of lattice mismatch. After an adequate time period (~2 ns), the atoms rearranged themselves to, presumably, their lowest energy state, and formed a semi-coherent or a relaxed interface to accommodate the disparity between lattice parameters. Even though periodic boundary conditions are imposed along the planes perpendicular to the interface to simulate an infinite film, the structure experiences the spatial

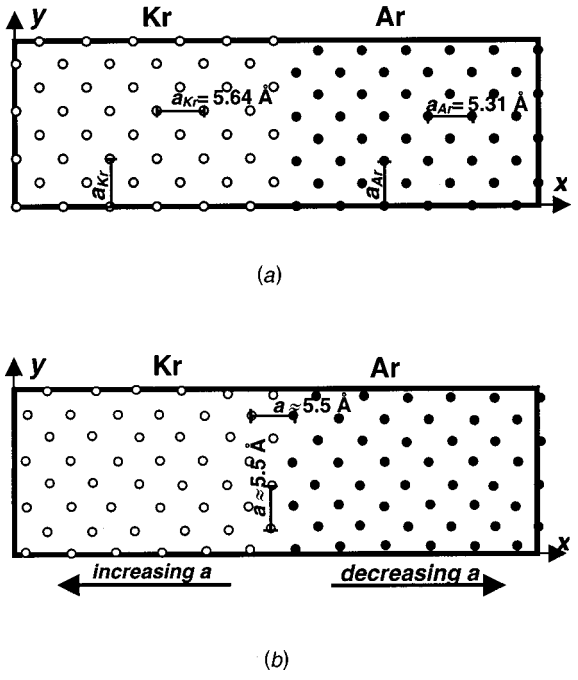

Fig. 6 (*a*) initial and (*b*) final positions of Kr (light circles) and Ar (dark circles) atoms for a molecular dynamics simulation of a bi-material film with a semi-coherent or relaxed interface. The initial conditions are set to the exact lattice parameters of Kr and Ar. After the simulation, the atoms rearranged themselves such that the lattice parameter at the interface is approximately the average of a_{Kr} and a_{Ar}. The interatomic distance grows smaller for the Ar atoms and larger for the Kr atoms away from the interface.

constraints of the relatively small dimensions of the simulation. Consequently, it is favorable for the atomic spacing on either side of the interface to either slightly contract (Kr atoms) or expand (Ar atoms) to align with adjacent atoms, while the atoms farthest away from the interface maintain their respective lattice parameters. Since the structure exhibits a smooth transition from the Kr to Ar film, the interfacial strain is minimized and there is relatively no lattice strain in either film just a few atomic planes away from the interface. This behavior is similar to what one would expect at the interface between heterostructures of nanowires in which there are only a relatively small number of atoms along the interface as opposed to in an actual superlattice where an interface may consist of many millions of atoms.

The thermal conductivities of bi-material structures with relaxed interfaces and of differing overall thicknesses are compared with their strained counterparts and calculated average thermal conductivities in Fig. 7. The strained and average values for the thermal conductivity come directly from Fig. 3. The probable error of the effective thermal conductivity for the unstrained case is approximately 10 percent for all structures. The results demonstrate that for the MD simulations, allowing the two materials to exist in their natural lattice state rather than forcing a coherent interface results in an increase in thermal conductivity. In fact, the effective thermal conductivity of the strained structure is ~35 percent lower than when the entire structure is in a relaxed state. Using the thermal conductivity results from the strained and relaxed simulations along with the average calculation for the films given by Eq. (3), the boundary resistance (BR) for both the strained and relaxed cases can be determined and compared using a simple series resistance relationship, $R_{\text{eff}}=R_{\text{Kr}}+R_{\text{Ar}}+R_{\text{BR}}$. Consequently, the boundary resistance in the case of the strained structure is calculated to be more than three times that of the relaxed structure. Not only does strain throughout the Ar film

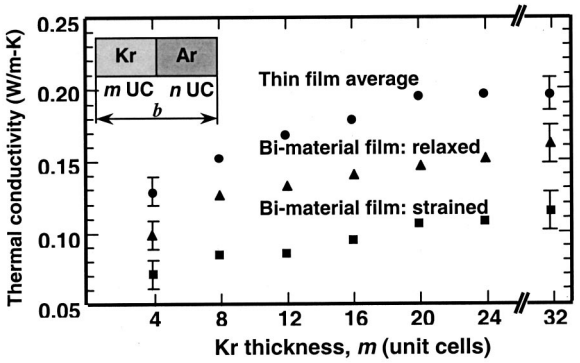

Fig. 7 Effective thermal conductivity of bi-material Kr/Ar films as a function of overall thickness (thickness ratio=1) for strained (solid square), relaxed (solid triangle) and thin film average (solid circle) cases. Note $m=n$.

result in a decrease in effective thermal conductivity, but the property mismatch that results from the strain also appears to contribute to a further reduction. Comparing the three trends in Fig. 7, it seems that the strain due to forcing a coherent interface may actually be a dominant contributor to the reduction in thermal conductivity. Reflection due to other mechanisms may only result in a reduction of ~20 percent of the average thermal conductivity value as compared to a reduction of ~50 percent for the strained heterostructures.

Performing a simple calculation to estimate the influence of lattice strain on the thermal conductivity provides elementary insight to the degree of its effect. Taking the second derivative of the interatomic potential [Eq. (2)] gives the spring stiffness, $g = d^2\Phi/dr_{ij}^2$ of the interatomic bond. Forcing the Ar film in tension to match the lattice constant of Kr, results in a strain, $\gamma=(a_s - a_0)/a_0=6.2$ percent experienced throughout the Ar film. For this calculation, a_s is the strained lattice constant, or in this case the lattice constant corresponding to Kr, and a_0 is the equilibrium lattice constant, or the natural lattice constant of Ar. The expression for the spring stiffness as a function of lattice strain is derived for the L-J potential to be

$$g = g_0\left[\frac{13}{6}\frac{1}{(1+\gamma)^{14}} - \frac{7}{6}\frac{1}{(1+\gamma)^{8}}\right] \tag{4}$$

where the spring stiffness at equilibrium, $g_0=72\varepsilon/2^{1/3}\sigma^2$. Because of anharmonicity in the interatomic potential, the spring stiffness of the strained lattice will be different from that of the relaxed state, and for $\gamma=6.2$ percent, $g/g_0=0.21$.

The change in spring stiffness fundamentally alters the phonon dispersion relation, which in turn modifies the phonon group velocity as well as the lifetime of phonon-phonon interaction, τ_{ph}. The effect of both these contributions to thermal conductivity can be significant. As a demonstration, consider only the effect of modifying the phonon group velocity and disregard a change in τ_{ph}. Then, applying kinetic theory and substituting the velocity, $v \approx r_{ij}\sqrt{g/m}$, into the expression for thermal conductivity,

$$k = \frac{1}{3}Cr_{ij}^2\frac{g}{m}\tau_{ph} \tag{5}$$

where C is heat capacity. Using the above expressions, the thermal conductivity of the relaxed Ar film is reduced by ~80 percent when a strain of 6.2 percent is imposed. However, molecular dynamics simulations of single Ar films in the strained and relaxed states revealed a reduction of only ~30 percent in thermal conductivity.

Conclusions

There is limited understanding of the many complex mechanisms affecting thermal transport in heterostructures with one or multiple interfaces. This study served to assess the feasibility of using molecular dynamics as a tool to further elucidate the effects of varying parameters in these types of structures such as overall thickness and the ratio of the respective material composition, the number of interfaces per unit length, and lattice strain. The results indicate that for simple asymmetrically strained bi-material films where a single interface is present, the thermal conductivity may be less than half the value of an average of two similar thin films. Moreover, one would expect that varying the ratio of the two materials in a simple bi-material film would also affect thermal transport, particularly if the thermal conductivities of the two materials are markedly different. However, when one or both of the films approach the phonon mean free path, the possible competing effects of thin film boundary scattering and the ratio of film composition must be considered. Nonetheless, there is no conclusive evidence from this study that variation in the ratio of the constituent materials significantly influences interfacial thermal effects. There are competing theories that suggest that increasing the number of interfaces per unit length will influence the thermal conductivity of the structure. However, this study demonstrated that a single interface results in a considerable decrease in thermal conductivity, but additional interfaces do not necessarily cause a further significant reduction in the property. Care must be taken to account for the competing increase in effective thermal conductivity due to phonon tunneling in superlattices with thin films of the order of or less than the dominant phonon wavelength, and it is important to also examine whether mini-band formation might be present to counteract phonon reflection at the interface. In one of the first investigations into the effect of lattice strain on thermal conductivity in heterostructures, this study revealed that the imposed tensile strain caused by forcing a coherent interface resulted in a significant decrease in the thermal conductivity. A more accurate theoretical analysis must quantify the effects of the imposed strain on the dispersion relation and phonon relaxation time before a thorough understanding of its effects on thermal conductivity can be fully appreciated. Nonetheless, results provide some insight into the mechanisms that may influence thermal transport, and should be carefully considered in the design of superlattices used for the purpose of manipulation of heat flow.

Acknowledgments

The authors gratefully acknowledge the financial support of the National Science Foundation and the Department of Energy.

Nomenclature

Ar = argon
C = specific heat (J/kg-K)
Kr = krypton
M = total number of planes
N_x = atomic plane number at location x
R = thermal resistance (K/W)
T_x = atomic plane temperature at location x
a = lattice constant (○)
b = slope
g = spring stiffness (N/m)
k = thermal conductivity (W/m-K)
k_B = Boltzmann's constant (1.38×10^{-23} J/K)
m = mass (kg)
q = heat flux (W/m^2)
r_{ij} = distance between atoms i and j
t = thickness (m)
v = velocity (m/s)

Greek Symbols

ε = well-depth parameter (J)

γ = strain
Φ = interatomic potential (J)
σ = probable error
σ_{sd} = probable error
$\sigma_{\langle\ \rangle}$ = standard error
σ_{LJ} = Lennard-Jones equilibrium separation parameter (○)
τ_{ph} = phonon relaxation time (s)
τ_{run} = run time (s)
τ_{corr} = autocorrelation time (s)

Subscript

0 = equilibrium
BR = boundary resistance
eff = effective
f = film
inst = instantaneous
s = strained
x = plane number

Appendix

The error analysis of the effective thermal conductivity involves a series of calculations that examine the statistical fluctuations of the simulation. Lukes et al. [36] provide additional details of the error analysis. The standard deviation of the planar temperature, $\sigma_{sd,Tx}$, is first used to determine the standard error of the planar temperature [35,43],

$$\sigma_{\langle Tx\rangle} = \sigma_{sd,Tx}\sqrt{2\,\tau_{\mathrm{corr}}/\tau_{\mathrm{run}}} \tag{6}$$

where τ_{run} is the run time of the simulation after reaching steady state, and τ_{corr} is the autocorrelation time of the instantaneous planar temperatures given approximately by the ratio of phonon mean free path [39] to the speed of sound [44]. For simulations involving bi-material structures, the average of the speeds of sound is used. The probable error associated with the slope of the best fit line of the temperature profile of the regular atoms is found using a weighted least squares method [45],

$$\sigma_{b_f} = \sqrt{\frac{\left(\Sigma_{x=1}^{M_f}\frac{1}{\sigma_{\langle Tx\rangle}^2}\right)}{\left(\Sigma_{x=1}^{M_f}\frac{1}{\sigma_{\langle Tx\rangle}^2}\right)\left(\Sigma_{x=1}^{M_f}\frac{x^2}{\sigma_{\langle Tx\rangle}^2}\right)-\left(\Sigma_{x=1}^{M_f}\frac{1}{\sigma_{\langle Tx\rangle}^2}\right)^2}} \tag{7}$$

where x is the plane number along the x-direction and M_f is the total number of planes in the film. For bi-material films, the slope, b_f, and its respective error, σ_{bf}, are calculated for each individual film. For example, a structure composed of four alternating layers of Kr and Ar will require the calculation of the four different slopes and their respective errors. Each individual film's thermal conductivity, k_f, is also calculated as the quotient of the effective heat flux, q_{eff}, and the respective slope, b_f, to be used in subsequent error calculations. There will also be a probable error associated with the effective heat flux, q_{eff} [45],

$$\sigma_{q_{\mathrm{eff}}} = \sqrt{\left(\sum_{x=1}^{M}\sigma_{\langle q_x\rangle}^2\right)\frac{\partial q_{\mathrm{eff}}}{\partial\langle q_x\rangle}} \tag{8}$$

where $\sigma_{\langle qx\rangle}$ is the standard error of the planar heat flux, q_x, calculated for each plane along the x-direction in the same manner as Eq. (7). Finally, the formulation for the total probable error of each film's thermal conductivity is

$$\sigma_{k_f} = \sqrt{\sigma_{q_{\mathrm{eff}}}^2\left(\frac{\partial k_f}{\partial q_{\mathrm{eff}}}\right)^2+\sigma_{b_f}^2\left(\frac{\partial k_f}{\partial b_f}\right)^2} \tag{9}$$

The largest value of σ_{kf} from those calculated for each film is used to represent the probable error of the effective thermal conductivity of the bi-material structure.

References

[1] Mahan, G., Sales, B., and Sharp, J., 1997, "Thermoelectric materials: New Approaches to an Old Problem," Phys. Today, **50**, pp. 42–47.
[2] Dresselhaus, M. S., Dresselhaus, G., Sun, X., Zhang, Z., Cronin, S. B., Koga, T., Ying, J. Y., and Chen, G., 1999, "The Promise of Low-Dimensional Thermoelectric Materials," Microscale Thermophys. Eng., **3**, pp. 89–100.
[3] Yao, T., 1987, "Thermal Properties of AlAs/GaAs Superlattices," Appl. Phys. Lett., **51**, pp. 1798–1800.
[4] Weisbuch, C., and Vinter, B., 1991, *Quantum Semiconductor Structures*, Academic Press, Boston, MA.
[5] Capinski, W. S., and Maris, H. J., 1996, "Thermal Conductivity of GaAs/AlAs Superlattices," Physica B, **220**, pp. 699–701.
[6] Capinski, W. S., Maris, H. J., Ruf, T., Cardona, M., Ploog, K., and Katzer, D. S., 1999, "Thermal Conductivity Measurements of GaAs/AlAs Superlattices Using a Picosecond Optical Pump-and-Probe Technique," Phys. Rev. B, **59**, pp. 8105–8113.
[7] Lee, S. M., Cahill, D. G., and Venkatasubramanian, R., 1997, "Thermal Conductivity of Si-Ge Superlattices," Appl. Phys. Lett., **70**, pp. 2957–2959.
[8] Yamasaki, I., Yamanaka, R., Mikami, M., Sonobe, H., Mori, Y., and Sasaki, T., 1998, "Thermoelectric Properties of Bi_2Te_3 /Sb_2Te_3 Superlattice Structures," *Proceedings 17th International Thermoelectrics Conference ICT '98*, IEEE, CA, pp. 210–213.
[9] Venkatasubramanian, R., 2000, "Lattice Thermal Conductivity Reduction and Phonon Localization Like Behavior in Superlattice Structures," Phys. Rev. B, **61**, pp. 3091–3097.
[10] Huxtable, S. T., Abramson, A. R., Majumdar, A., Tien, C. L., LaBounty, C., Fan, X., Zeng, G., Abraham, P., Bowers, J. E., Shakouri, A., and Croke, E. T., 2001, "Thermal Conductivity of Si/SiGe Superlattices," *Proceedings IMECE '01*, ASME, New York.
[11] Chen, G., and Neagu, M., 1997, "Thermal Conductivity and Heat Transfer in Superlattices," Appl. Phys. Lett., **71**, pp. 2761–2763.
[12] Rosenblum, I., Adler, J., Brandon, S., and Hoffman, A., 2000, "Molecular-Dynamics Simulation of Thermal Stress at the (100) Diamond/Substrate Interface: Effect of Film Continuity," Phys. Rev. B, **62**, pp. 2920–2936.
[13] Borca-Tasciuc, T., Achimov, D., Liu, W. L., Chen, G., Lin, C. H., Delaney, A., and Pei, S. S., 2001, "Thermal Conductivity of InAs/AlSb Superlattices," *Proceedings International Conference on Heat Transfer and Transport Phenomena in Microscale*, Banff, Canada, Begell House, New York, pp. 369–371.
[14] Borca-Tasciuc, T., Liu, W. L., Liu, J. L., Zeng, Song, D. W., Moore, C. D., Chen, G., Wang, K. L., Goorsky, M. S., Radetic, T., Gronsky, R., Sun, X., and Dresselhaus, M. S., 1999, "Thermal Conductivity of Si/Ge Superlattices," *Proceedings 18th International Conference on Thermoelectrics ICT '99* IEEE, CA.
[15] Rieger, M. M., and Vogl, P., 1993, "Electronic-Band Parameters in Strained Si(1-x)Ge(x) Alloys on Si(1-y)Ge(y) Substrates," Phys. Rev. B, **48**, pp. 14276–14287.
[16] Tserbak, C., Polataoglou, H. M., and Theodorou, G., 1993, "Unified Approach to the Electronic-Structure of Strained Si/Ge Superlattices," Phys. Rev. B, **47**, pp. 7104–7124.
[17] Ghanbari, R. A., White, J. D., Fasol, G., Gibbings, C. J., and Tuppen, C. G., 1990, "Phonon Frequencies for Si-Ge Strained Layer Superlattices Calculated in a Three-Dimensional Model," Phys. Rev. B, **42**, pp. 7033–7041.
[18] Qteish, A., and Molinari, E., 1990, "Interplanar Forces and Phonon Spectra of Strained Si and Ge: *Ab initio* Calculations and Applications to Si/Ge Superlattices," Phys. Rev. B, **42**, pp. 7090–7096.
[19] Sui, Z., and Herman, I. P., 1993, "Effect of Strain on Phonons in Si, Ge, and Si/Ge Heterostructures," Phys. Rev. B, **48**, pp. 17938–17953.
[20] Little, W. A., 1959, "The Transport of Heat Between Dissimilar Solids at Low Temperatures," Can. J. Phys., **37**, pp. 334–349.
[21] Stoner, R. J., and Maris, H. J., 1993, "Kapitza Conductance and Heat Flow Between Solids at Temperatures From 50 to 300 K," Phys. Rev. B, **48**, pp. 16373–16387.
[22] Tamura, S., Tanaka, Y., and Maris, H. J., 1999, "Phonon Group Velocity and Thermal Conduction in Superlattices," Phys. Rev. B, **60**, pp. 2627–2630.
[23] Tamura, S., Hurley, D. C., and Wolfe, J. P., 1988, "Acoustic Phonon Propagation in Superlattices," Phys. Rev. B, **38**, pp. 1427–1449.
[24] Simkin, M. V., and Mahan, G. D., 2000, "Minimum Thermal Conductivity of Superlattices," Phys. Rev. Lett., **84**, pp. 927–930.
[25] Narayanamurti, V., Stormer, H. L., Chin, M. A., Gossard, A. C., and Wiegmann, W., 1979, "Selective Transmission of High-Frequency Phonons by a Superlattice: The "Dielectric" Phonon Filter," Phys. Rev. Lett., **43**, pp. 2012–2016.
[26] Chen, G., 1999, "Phonon Wave Heat Conduction in Thin Films and Superlattices," ASME J. Heat Transfer, **121**, pp. 945–953.
[27] Swartz, E. T., and Pohl, R. O., 1987, "Thermal Resistance at Interfaces," Appl. Phys. Lett., **51**, pp. 2200–2202.
[28] Balandin, A., and Wang, K. L., 1998, "Significant Decrease of the Lattice Thermal Conductivity Due to Phonon Confinement in a Free-Standing Semiconductor Quantum Well," Phys. Rev. B, **58**, pp. 1544–1549.
[29] Chen, G., 1997, "Size and Interface Effects on Thermal Conductivity of Superlattices and Periodic Thin-Film Structures," ASME J. Heat Transfer, **119**, pp. 220–229.
[30] Chen, G., 1998, "Thermal Conductivity and Ballistic-Phonon Transport in the Cross-Plane Direction of Superlattices," Phys. Rev. B, **57**, pp. 14958–14973.
[31] Peterson, R. B., 1994, "Direct Simulation of Phonon-Mediated Heat Transfer in a Debye Crystal," ASME J. Heat Transfer, **116**, pp. 815–1994.

[32] Mazumdar, S., and Majumdar, A., 2001, ''Monte Carlo Study of Phonon Transport in Solid Thin Films Including Dispersion and Polarization,'' ASME J. Heat Transfer, **123**, pp. 749–759.
[33] Liang, X. G., and Shi, B., 2000, ''Two-Dimensional Molecular Dynamics Simulation of the Thermal Conductance of Superlattices,'' Mater. Sci. Eng., A, **292**, pp. 198–202.
[34] Volz, S., Saulnier, J. B., Chen, G., and Beauchamp, P., 2000, ''Molecular Dynamics of Heat Transfer in Si/Ge Superlattices,'' High Temp.-High Press., **32**, pp. 709–714.
[35] Allen, M. P., and Tildesley, D. J., 1987, *Computer Simulation of Liquids*, Clarendon Press, Oxford.
[36] Lukes, J. R., Li, D. Y., Liang, X. G., and Tien, C. L., ''Molecular Dynamics Study of Solid Thin-Film Thermal Conductivity,'' ASME J. Heat Transfer, **122**, pp. 536–543.
[37] Irving, J. H., and Kirkwood, J. G., 1950, ''The Statistical Mechanical Theory of Transport Processes A. The Equations of Hydrodynamics,'' J. Chem. Phys., **18**, pp. 817–829.
[38] Swope, W. C., Anderson, H. C., Berens, P. H., and Wilson, K. R., 1982, ''A Computer Simulation Method for the Calculation of Equilibrium Constants for the Formation of Physical Clusters of Molecules: Application to Small Water Clusters,'' J. Chem. Phys., **76**, pp. 637–649.
[39] Dobbs, E. R., and Jones, G. O., 1957, ''Theory and Properties of Solid Argon,'' Rep. Prog. Phys., **20**, pp. 516–564.
[40] Reid, R. C., Prausnitz, J. M., and Poling, B. E., 1987, *The Properties of Gases and Liquids*, Mc-Graw Hill, New York.
[41] White, G. K., and Woods, S. B., 1958, ''Thermal Conductivity of the Solidified Inert Gases: Argon, Neon and Krypton,'' Philos. Mag., **3**, pp. 785–797.
[42] Bao, Y., and Chen, G., 2000, ''Lattice Dynamics Study of Anisotropy of Heat Conduction in Superlattices,'' *Proceedings of MRS Spring Meeting, Symposium Z*, Materials Research Society, PA.
[43] Jacucci, G., and Rahman, A., 1984, ''Comparing the Efficiency of Metropolis Monte Carlo and Molecular Dynamics Methods for Configuration Space Sampling,'' Nuovo Cimento, **D4**, pp. 341–356.
[44] Weast, R. C., Astle, M. J., and Beyer, W. H., eds., 1996, *CRC Handbook of Chemistry and Physics*, CRC Press, Boca Raton.
[45] Press, W. H., Teukolsky, S. A., Vetterling, W. T., and Flannery, B. P., 1992, *Numerical Recipes in FORTRAN: The Art of Scientific Computing*, 2nd edition, Cambridge University Press, Cambridge.